ЖЭТФ, 2022, том 162, вып. 4 (10), стр. 555–563

MOMENTUM ALIGNMENT AND THE OPTICAL VALLEY HALL EFFECT IN LOW-DIMENSIONAL DIRAC MATERIALS

V. A. Saroka [a,b], ***R. R. Hartmann*** [c], ***M. E. Portnoi*** [a*]

[a] *Physics and Astronomy, University of Exeter, Stocker Road, Exeter EX4 4QL, United Kingdom*

[b] *Institute for Nuclear Problems, Belarusian State University, 220030, Minsk, Belarus*

[c] *Physics Department, De La Salle University, 0922 Manila, Philippines*

Received June 2, 2022,
revised version June 9, 2022
Accepted June 10, 2022

Contribution for the JETP special issue in honor of E. I. Rashba's 95th birthday

DOI: 10.31857/S004445102210011X
EDN: JTNVUO

One of the best-known properties of graphene is its universal optical absorption for a broad range of frequencies [1]. It is less-known that a linearly polarized excitation creates in graphene-like materials a strongly anisotropic distribution of photoexcited carriers, with their momenta aligned preferentially normal to the polarization plane, allowing one to effectively steer the direction of electrons by light [2]. This largely overlooked effect is the central theme of our paper. A similar momentum alignment phenomenon occurs in bulk GaAs-type semiconductors [3] and quantum wells [4–8], where the electrons created by the interband absorption of linearly polarized light are also distributed anisotropically in momentum space; the same selection rules govern polarization properties of quantum-well-based lasers [9]. In conventional semiconductors the alignment is due to the spin-orbit interaction, whereas in graphene, it is due to the pseudo-spin. Namely, the ratio of the two components of the spinor-like graphene wavefunction depends on the direction of momentum which influences the optical transition selection rules. Unlike semiconductors where most optical phenomena are associated with the band edge transitions, photoexcited carriers in graphene are always created with a significant value of momentum and a linearly polarized excitation results in strong momentum anisotropy for all excitation energies. Momentum alignment in graphene was first discussed in Ref. [2] followed by a number of papers mostly dealing with the photogalvanic effect see, e. g., Ref. [10] and references therein. Notably, in this paper we do not deal with photocurrents largely influenced by relaxation processes [11], rather, we focus on the selection rules and the shape of the momentum distribution function at the instant of photoexcitation.

In graphene and graphene-like two-dimensional (2D) Dirac materials, such as single layers of group-VI dichalcogenides [12, 13] and elemental analogues of graphene [14,15] including silicene, germanene, stanene and several others, the electronic properties can be described in terms of particles belonging to two valleys [16], centered around the symmetry points **K** and **K′**. These points are nonequivalent and degenerate in terms of energy. This degree of degeneracy is the so-called valley degree of freedom. It has been proposed that this additional quantum number can be utilized in an analogous manner to spin in semiconductor spintronics [17] and has been suggested as a basis for carrying information in graphene-based devices [18]. For gapped 2D Dirac materials, excitation by linearly polarized light with a photon energy just above the band gap results in an equal population of both valleys. However, as we show below, at higher excitation energies, the trigonal warping effect (an anisotropy of the equal-energy contour) in conjunction with momentum alignment can be utilized to spatially separate carriers belonging to different valleys, thus providing a route to optovalleytronics — the optical control of valley population. This optical valley Hall effect becomes stronger as the photon energy increases.

* E-mail: M.E.Portnoi@exeter.ac.uk

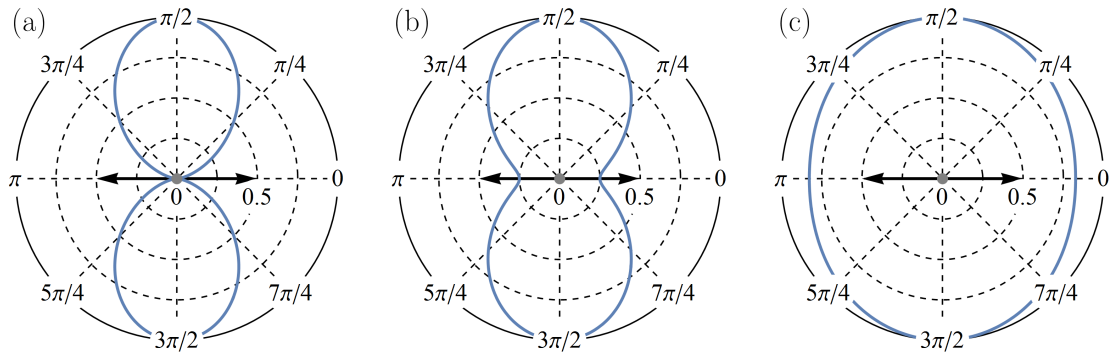

Fig. 1. The polar plots of the momentum distribution functions for (*a*) graphene and an isotropic gapped 2D Dirac material excited at (*b*) $h\nu = 2E_g$ and (*c*) $h\nu = 1.1E_g$, for $\phi = 0$. Here, the black arrow represents the polarization of the excitation, which is assumed to be along the x-axis

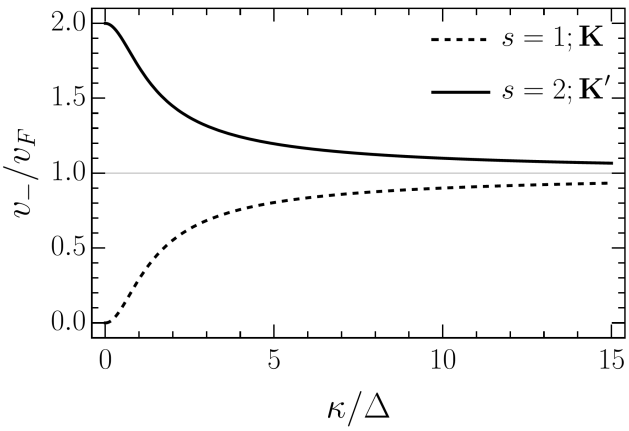

Fig. 2. The absolute value of the matrix element of the velocity operator associated with interband transitions induced by right-handed circularly polarized light as a function of excitation energy. The lower and upper curves correspond to the $\mathbf{K}$ and $\mathbf{K}'$ valleys, respectively

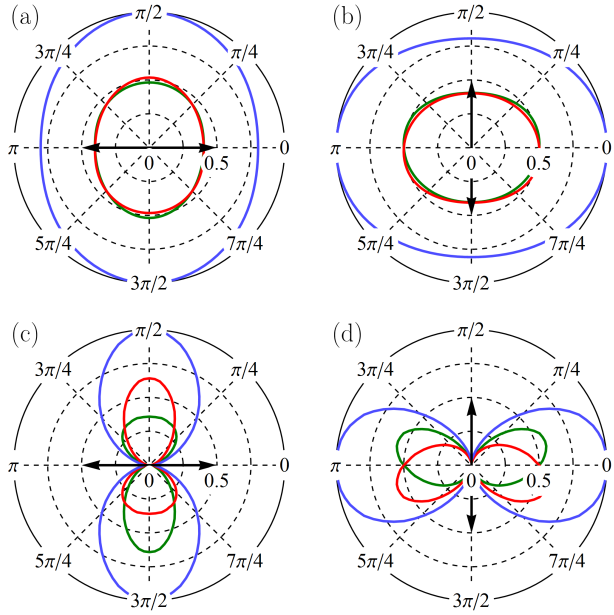

Fig. 3. The polar plots of the momentum distribution function of photoexcited carriers generated by linearly-polarized light in a gapped graphene-like crystal when the trigonal warping is taken into account for: (*a*) $\phi = 0$, $h\nu = 1.1E_g$, and $E_g = 0.1|t|$, (*b*) $\phi = \pi/2$, $h\nu = 1.1E_g$, and $E_g = 0.1|t|$, (*c*) $\phi = 0$, $h\nu = 5E_g$, and $E_g = 0.1|t|$, (*d*) $\phi = \pi/2$, $h\nu = 5E_g$, and $E_g = 0.1|t|$. Here, ϕ is the angle between the excitation polarization plane and the x-axis at normal light incidence. The energy gap is given in terms of the hopping integral, $|t| \approx 3$ eV. The green and red lines show the contributions from the $\mathbf{K}$ and $\mathbf{K}'$ valleys, respectively, while the blue contour is their sum, and the bold black arrows represent the polarization of the excitation

In gapless 2D materials, such as graphene, in addition to the aforementioned trigonal warping which occurs at high energies, there is a strong anisotropic modification to the spectra near the apex of the Dirac cone due to the celebrated Rashba spin-orbit effect [19–21], which is inevitable in the presence of a substrate and can be controlled by the back-gate voltage. The importance of Rashba spin-orbit interaction for graphene physics was realized by Kane and Mele [22] practically simultaneously with graphene exfoliation which was followed by an extensive body of research including important contributions by Rashba himself [23–25]. The presence of the Rashba term, which is significant at low energies, should result in an optical valley Hall effect occurring also at much lower far-infrared frequencies.

In contrast to the optical spin and valley Hall effects in polaritonics [26–28], our predicted optical valley Hall effect, caused by the spatial separation of carriers be-

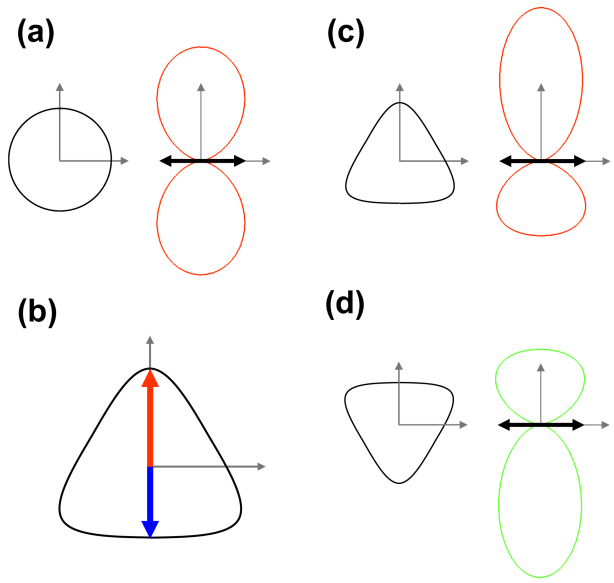

Fig. 4. (*a*) The polar plots of the momentum distribution of photo-excited carriers in the low-energy regime at normal light incidence when the excitation polarization plane is along the x-axis, i. e. $\phi = 0$. (*b*) The equienergy contour around the $\mathbf{K}'$ point (black line), in the regime where trigonal warping becomes important. Here, the red line indicates a direction in k-space where κ is maximum, while the blue line indicates a direction in k-space where κ is minimum. The contribution to the momentum distribution of photo-excited carriers from the (*c*) $\mathbf{K}'$ point and (*d*) $\mathbf{K}$ point is shown. In both instances $\phi = 0$ and $h\nu = 0.6|t|$. As a guide to the eye, the corresponding equienergy contours are drawn next to each distribution function and the bold black arrows represent the polarization of the excitation

longing to different valleys by linearly polarized light, does not need a microcavity. A better-known alternative route to optovalleytronics utilizes circularly polarized light in quasi-2D Dirac materials with non-zero effective mass. Unlike in gapless 2D Dirac materials, the selection rules for interband transitions for circularly polarized light in gapped graphene-like systems are strongly valley dependent. Namely, circularly polarized radiation of a specific handedness, with an energy matching the band gap, will excite electrons in one valley only. These optical transition selection rules are independent of the physical nature of the gap. The gap can be opened, e. g., by placing graphene on a matching substrate with two chemically different atoms underneath the two neighbouring carbon atoms [29,30] or chemically-functionalized graphene [31]. The valley-dependent selection rules for circularly-polarized light can be utilized for the detection of the optical valley Hall effect. In single layers of transition metal dichalcogenides [32] the gap is believed to be of a mixed nature, involving significantly differing on-site energies accompanied by spin-valley locking due to strong spin-orbit coupling. Thus, in these materials the optical valley Hall effect is automatically accompanied by the optical spin Hall effect.

The momentum alignment phenomenon also has profound consequences for optical transition selection rules in narrow-gap carbon nanotubes (CNTs) and graphene nanoribbons (GNRs). Namely, the angular dependence of graphene's momentum distribution function leads to a spectacular enhancement in the matrix element of optical interband transition at the band edge in these quasi-one-dimensional (1D) nanostructures. This enhancement is due to an effective quantized momentum in the direction normal to the CNT or GNR axis which governs the interband transitions when the free momentum along the axis is small. The pronounced peak in the optical matrix element at the band gap edge has a universal value which is proportional to the Fermi velocity and is independent of nature of the gap, which can be magnetic-field, curvature or edge-effect induced.

In what follows, we derive the optical selection rules for interband transitions in 2D Dirac materials for both linearly and circularly polarized excitations. In the low-energy regime and in the absence of the Rashba term, the optical selection rules for linearly-polarized excitations are shown to be valley independent; the same is true for circularly-polarized excitations in graphene. In contrast, for gapped 2D Dirac materials the optical transitions associated with circularly-polarized light are valley-dependent. The distribution of photoexcited carriers is first calculated in the absence of the Rashba term, for both the low energy regime and for the range of frequencies in which trigonal warping effects become important. Next, we show that in the presence of warping, a linearly polarized excitation will result in the spatial separation of carriers belonging to different valleys (optical valley Hall effect). An experimental set up is proposed to observe this effect in gapped 2D Dirac materials.

We then return to the low-energy part of the spectrum of gapless materials, but with the Rashba term introduced. This term results in a strong warping effect near the apex of the Dirac cone. This leads to a spectacular valley separation effect upon a linearly-polarized excitation, at a completely different photon energy scale. This energy scale can be tuned by modifying the strength of the Rashba term by changing the value of the back-gate voltage.

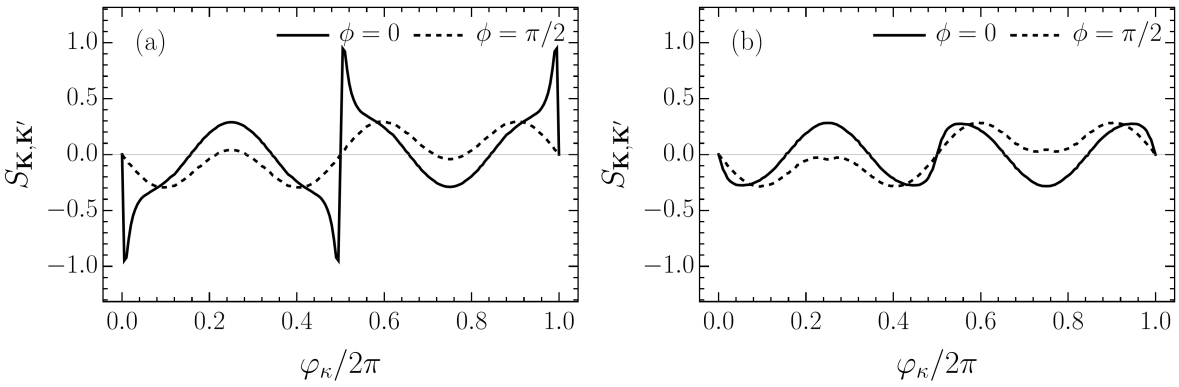

Fig. 5. The degree of valley polarization for (*a*) $E_g = 0$ and (*b*) $E_g = 0.1|t|$ for an excitation frequency of $h\nu = 0.5|t|$. The solid and dashed lines correspond to the polarization angles $\phi = 0$ and $\phi = \pi/2$ respectively

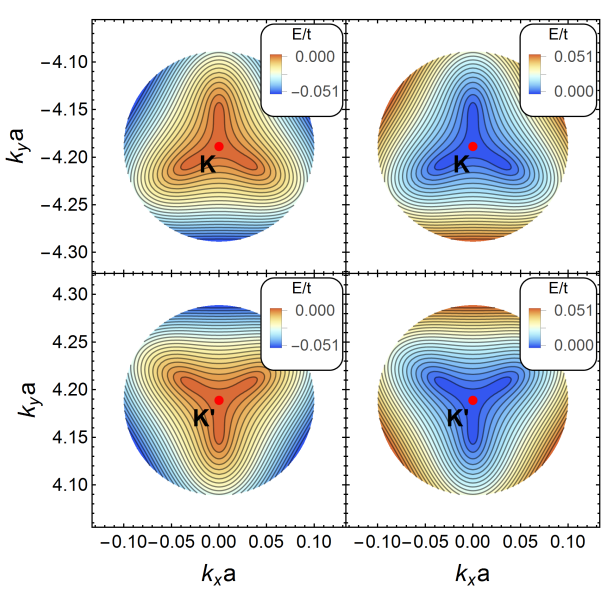

Fig. 6. The graphene valence and conduction energy bands around the $\mathbf{K}$ and $\mathbf{K}'$ points when Rashba spin-orbit interaction is accounted for. The Rashba coupling constant is chosen to be $\lambda_R = 0.1|t|$ in terms of the hopping integral, t

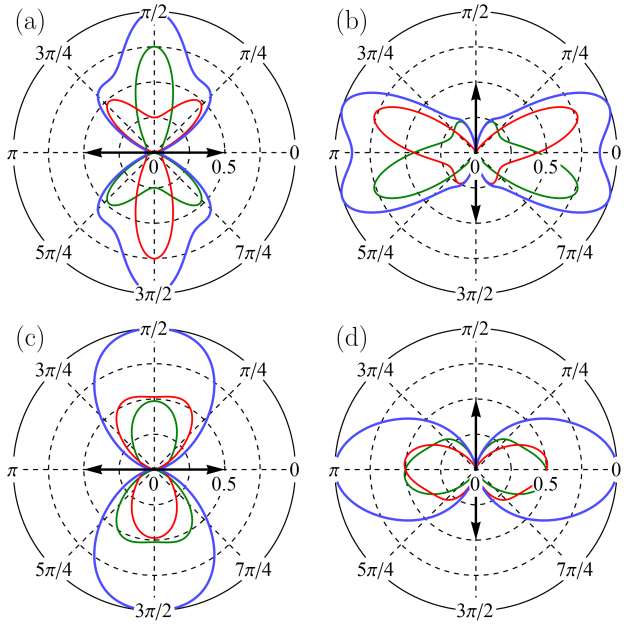

Fig. 7. The polar plots of the momentum distribution function of photoexcited carriers generated by linearly-polarized light in graphene when Rashba spin-orbit coupling is taken into account: (*a*) $\phi = 0$ and $h\nu = 0.05|t|$, (*b*) $\phi = \pi/2$ and $h\nu = 0.05|t|$, (*c*) $\phi = 0$ and $h\nu = 0.3|t|$, (*d*) $\phi = \pi/2$ and $h\nu = 0.3|t|$. Here ϕ is the angle between the excitation polarization plane and the x-axis assuming normal incidence. The Rashba coupling constant is chosen to be $\lambda_R = 0.1|t|$, where $|t| \approx 3$ eV is the hopping integral in graphene. The green and red lines show the contributions from the $\mathbf{K}$ and $\mathbf{K}'$ valley, respectively; while the blue contour is the total sum of valley contributions. The bold black arrows represent the polarization of the excitation

We also apply the theory of momentum alignment in graphene to quasi-1D systems such as narrow-gap CNTs and armchair GNRs (AGNRs). These systems are shown to have strong low-energy interband transitions, which are typically in the THz range [33]. Finally, we discuss the possibility for the experimental observation of the predicted strong THz transitions and how they could be used in THz emitters.

The results from the list of Refs. [1–92] are used and/or discussed in our work. The presented figures illustrate our results.

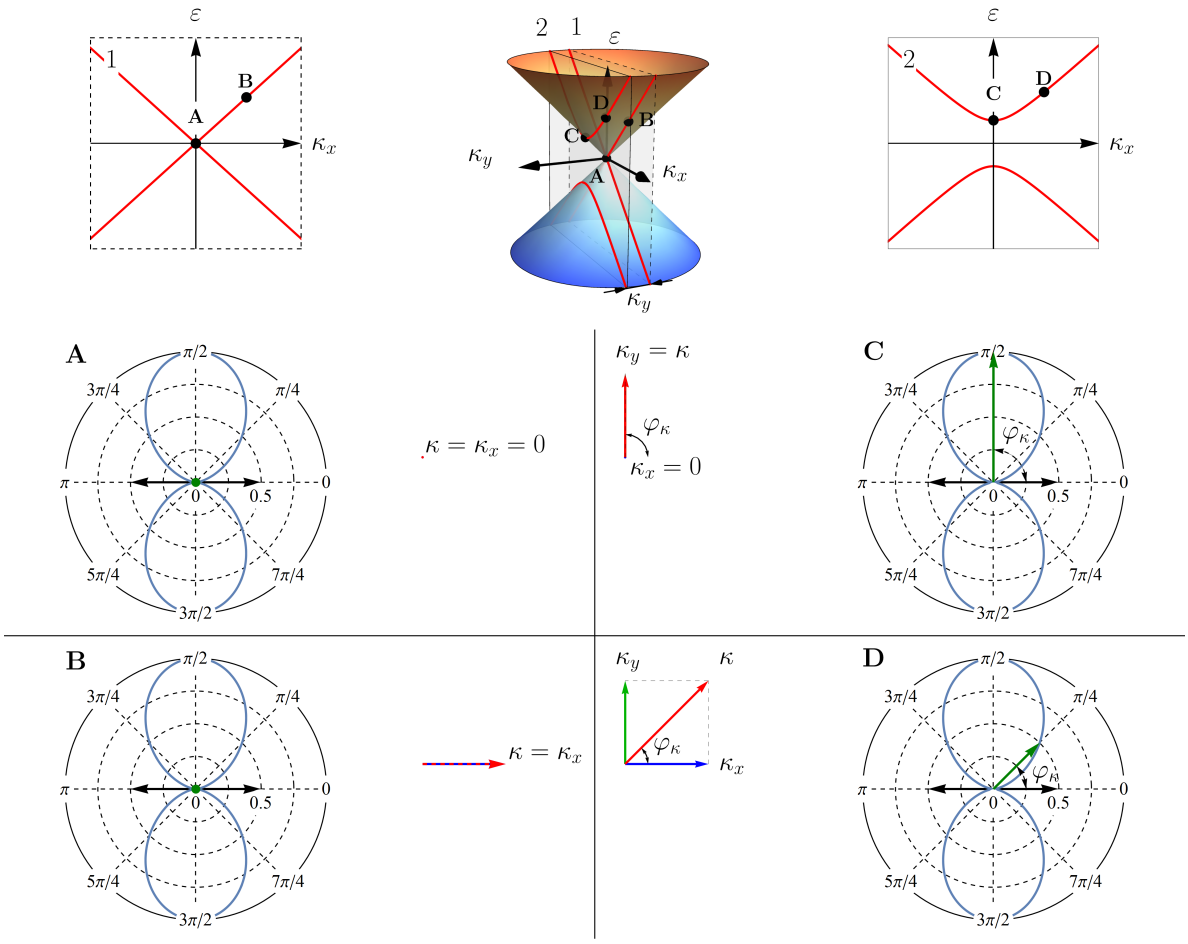

Fig. 8. Illustration of the giant enhancement of interband transitions across the narrow band gap in quasi-metallic carbon nanotubes and graphene nanoribbons explained in terms of the momentum alignment phenomenon in graphene. Each of the panels A, B, C, and D shows the dependence of the transition matrix element on the angle between the excitation polarization plane and the momentum of the photoexcited carrier, as well as the momentum vector direction. A and B correspond to the gapless case with the energy spectrum shown in the top left-hand side panel when the cross section of the cone passes through the Dirac point ($\kappa_y = 0$). As there is no momentum normal to the light polarization plane, optical transitions are totally forbidden in the conic approximation for both A ($\kappa_x = 0$) and B ($\kappa_x \neq 0$). C and D correspond to the narrow-gap case when the cross section avoids the Dirac point ($\kappa_y \neq 0$). C is for a band-edge transition when $\kappa_x = 0$ and the transition probability reaches its maximum. D corresponds to $\kappa_y \neq 0$ and $\kappa_x \neq 0$, the increase in κ_x leads to a reduction in the transition probability. The length of the dark-green arrows in the polar plots (vanishing for A and B) show the magnitude of the matrix element of transition

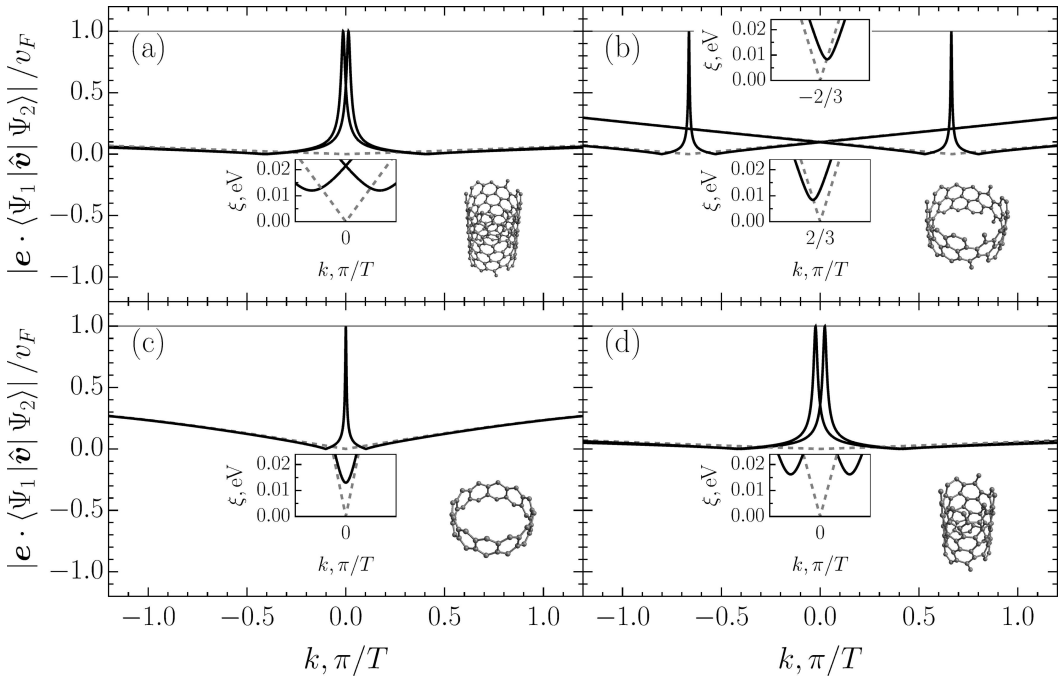

Fig. 9. The absolute value of the velocity operator matrix element with (solid black) and without (dashed grey) curvature effect for (*a*) CNT $(9,3)$; (*b*) CNT $(12,3)$; (*c*) CNT $(12,0)$, and (*d*) CNT $(6,3)$. The insets show the conduction bands in the vicinity of the Dirac point with (solid black) and without (dashed grey) curvature effect taken into account. The CNT unit cells are presented in the bottom right corner of each plot. For all chosen tubes, only the C–C bond contraction which dominates the curvature effects is accounted for. The universal character of the peak is highlighted by the solid horizontal line which marks v_F level. T is the translation period of the tube

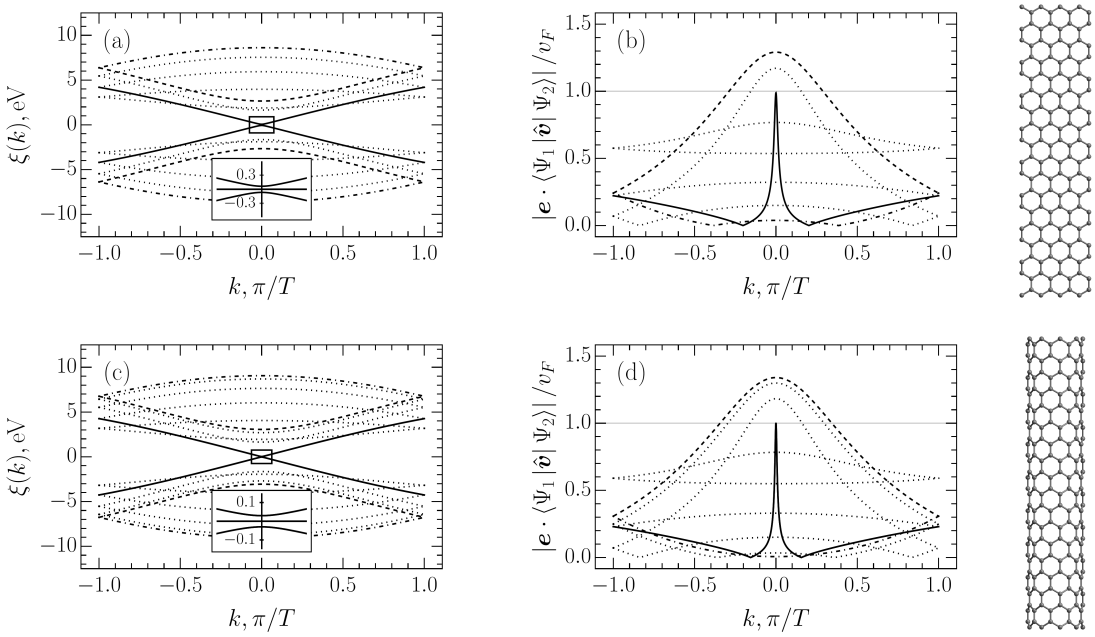

Fig. 10. (*a*),(*c*) are the band structures and (*b*), (*d*) are the velocity operator matrix elements of a AGNR(8) and zigzag CNT$(9,0)$, respectively. Transitions between the closest valence and conduction subbands (thick black line), the lowest and highest subbands (dashed dotted, light gray line), and for the subbands, for which velocity matrix element attains the maximum possible value (dashed, gray line), are highlighted with respect to the remaining bands and matrix elements (gray, dotted line). The insets in panels (*a*) and (*c*) show the zoomed in region close to the Dirac point where the band gap is present. In panels (*b*) and (*d*) the solid horizontal line corresponds to v_F as a guide to the eye. On the right side the atomic structures are shown. In both cases the hopping integral, $|t| \approx 3$ eV and the edge correction for the ribbon is $0.05|t|$, whereas the curvature correction for the tube is $0.01|t|$. T is the translation period of the structure

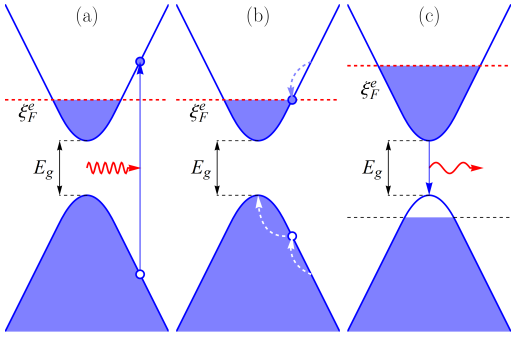

Fig. 11. A schematic illustration of (*a*) the high frequency optical excitation (*b*) non-radiative electron relaxation due to the electron-phonon scattering and (*c*) the population inversion in an n-doped narrow gap CNT or GNR

The full text of this paper is published in the English version of JETP.

REFERENCES

1. R. R. Nair, P. Blake, A. N. Grigorenko, K. S. Novoselov, T. J. Booth, T. Stauber, N. M. Peres, and A. K. Geim, Science **320**, 1308 (2008).
2. R. R. Hartmann and M. E. Portnoi, *Optoelectronic Properties of Carbon-based Nanostructures: Steering Electrons in Graphene by Electromagnetic Fields*, LAP Lambert Acad. Publ., Saarbrucken (2011); R. R. Hartmann, Ph. D. Thesis, Univ. of Exeter (2010).
3. D. N. Mirlin, in *Optical Orientation*, ed. by F. Meier and B. P. Zakharchenya, North Holland, Amsterdam (1984) Ch. 4.
4. I. A. Merkulov, V. I. Perel', and M. E. Portnoi, Zh. Eksp. Teor. Fiz. **99**, 1202 (1991).
5. D. N. Mirlin and V. I. Perel', Semicond. Sci. Technol. **7**, 1221 (1992).
6. J. A. Kash, M. Zachau, M. A. Tischler, and U. Ekenberg, Phys. Rev. Lett. **69**, 2260 (1992).
7. M. E. Portnoi, Sov. Phys. Semicond. **25**, 1294 (1991).
8. V. I. Perel' and M. E. Portnoi, Sov. Phys. Semicond. **26**, 1185 (1992).
9. E. A. Avrutin, I. E. Chebunina, I. A. Eliachevitch, S. A. Gurevich, M. E. Portnoi, and G. E. Shtengel, Semicond. Sci. Technol. **8**, 80 (1993).
10. M. V. Durnev and S. A. Tarasenko, Phys. Rev. B **103**, 165411 (2021).
11. L. E. Golub, S. A. Tarasenko, M. V. Entin, and L. I. Magarill, Phys. Rev. B **84**, 195408 (2011).
12. D. Xiao, G.-B. Liu, W. Feng, X. Xu, and W. Yao, Phys. Rev. Lett. **108**, 196802 (2012).
13. A. Kormányos, G. Burkard, M. Gmitra, J. Fabian, V. Zólyomi, N. D. Drummond, and V. Fal'ko, 2D Mater. **2**, 022001 (2015).
14. S. Balendhran, S. Walia, H. Nili, S. Sriram, and M. Bhaskaran, Small **11**, 640 (2015).
15. Z. Ni, E. Minamitani, Y. Ando, and S. Watanabe, Phys. Rev. B **96**, 075427 (2017).
16. J. R. Schaibley, H. Yu, G. Clark, P. Rivera, J. S. Ross, K. L. Seyler, W. Yao, and X. Xu, Nature Rev. Mater. **1**, 16055 (2016).
17. J. F. I. Žutić and S. D. Sarma, Rev. Mod. Phys. **76**, 323 (2004).
18. A. Rycerz, J. Tworzydlo, and C. W. J. Beenakker, Nature Phys. **3**, 172 (2007).
19. E. I. Rashba, Sov. Phys. Solid State **2**, 1109 (1960).
20. Yu. A. Bychkov and E. I. Rashba, J. Phys. C: Sol. St. Phys. **17**, 6039 (1984).
21. G. Bihlmayer, O. Rader, and R. Winkler, New J. Phys. **17**, 050202 (2015).
22. C. L. Kane and E. J. Mele, Phys. Rev. Lett. **95**, 146802 (2005).
23. E. I. Rashba, Phys. Rev. B **79**, 161409 (2009).
24. F. Kuemmeth and E. I. Rashba, Phys. Rev. B **80**, 241409 (2009).
25. D. Marchenko, A. Varykhalov, M. Scholz, G. Bihlmayer, E. Rashba, A. Rybkin, A. Shikin, and O. Rader, Nature Commun. **3**, 1232 (2012).
26. A. Kavokin, G. Malpuech, and M. Glazov, Phys. Rev. Lett. **95**, 136601 (2005).
27. C. Leyder, M. Romanelli, J. P. Karr, E. Giacobino, T. C. Liew, M. M. Glazov, A. V. Kavokin, G. Malpuech, and A. Bramati, Nature Phys. **3**, 628 (2007).
28. O. Bleu, D. D. Solnyshkov, and G. Malpuech, Phys. Rev. B **96**, 165432 (2017).
29. G. Giovannetti, P. A. Khomyakov, G. Brocks, P. J. Kelly, and J. van den Brink, Phys. Rev. B **76**, 073103 (2007).

30. S. Y. Zhou, G.-H. Gweon, A. V. Fedorov, P. N. First, W. A. de Heer, D.-H. Lee, F. Guinea, A. H. Castro Neto, and A. Lanzara, Nature Mater. **6**, 770 (2007).

31. M. F. Craciun, I. Khrapach, M. D. Barnes, and S. Russo, J. Phys.: Condens. Matter **25**, 423201 (2013).

32. S. Manzeli, D. Ovchinnikov, D. Pasquier, O. V. Yazyev, and A. Kis, Nature Rev. Mater. **2**, 17033 (2017).

33. M. E. Portnoi, V. A. Saroka, R. R. Hartmann, and O. V. Kibis, in *2015 IEEE Comput. Soc. Annu. Symp. VLSI* (IEEE, 2015), p. 456.

34. R. Saito, G. Dresselhaus, and M. S. Dresselhaus, *Physical Properties of Carbon Nanotubes*, Imperial College Press, London (1998).

35. J. Sichau, M. Prada, T. Anlauf, T. J. Lyon, B. Bosnjak, L. Tiemann, and R. H. Blick, Phys. Rev. Lett. **122**, 046403 (2019).

36. W. Yao, D. Xiao, and Q. Niu, Phys. Rev. B **77**, 235406 (2008).

37. A. Mattausch and O. Pankratov, Phys. Rev. Lett. **99**, 076802 (2007).

38. C. C. Liu, H. Jiang, and Y. Ya, Phys. Rev. B **84**, 195430 (2011).

39. V. A. Saroka, M. V. Shuba, and M. E. Portnoi, Phys. Rev. B **95**, 155438 (2017).

40. A. B. Kuzmenko, E. van Heumen, F. Carbone, and D. van der Marel, Phys. Rev. Lett. **100**, 117401 (2008).

41. M. Koshino and T. Ando, Phys. Rev. B **77**, 115313 (2008).

42. V. Ryzhii, M. Ryzhii, and T. Otsuji, J. Appl. Phys. **101**, 083114 (2007).

43. T. Stauber, N. M. R. Peres, and A. K. Geim, Phys. Rev. B **78**, 085432 (2008).

44. M. E. Portnoi, Semiconductors **27**, 294 (1993).

45. D. S. Kainth, M. N. Khalid, and H. P. Hughes, Sol. St. Commun. **122**, 351 (2002).

46. I. A. Merkulov, V. I. Perel, and M. E. Portnoi, Superlattices Microstr. **10**, 371 (1991).

47. K. F. Mak, C. Lee, J. Hone, J. Shan, and T. F. Heinz, Phys. Rev. Lett. **105**, 136805 (2010).

48. X. Xu, W. Yao, D. Xiao, and T. F. Heinz, Nature Phys. **10**, 343 (2014).

49. E. McCann, K. Kechedzhi, V. I. Fal'ko, H. Suzuura, T. Ando, and B. L. Altshuler, Phys. Rev. Lett. **97**, 146805 (2006).

50. F. V. Tikhonenko, D. W. Horsell, R. V. Gorbachev, and A. K. Savchenko, Phys. Rev. Lett. **100**, 056802 (2008).

51. L. Brey and H. Fertig, Phys. Rev. B **73**, 235411 (2006).

52. M. I. D'yakonov and V. I. Perel', Sov. Phys. JETP Lett. **13**, 467 (1971).

53. M. I. Dyakonov and V. I. Perel', Phys. Lett. A **35**, 459 (1971).

54. J. Sinova, S. O. Valenzuela, J. Wunderlich, C. H. Back, and T. Jungwirth, Rev. Mod. Phys. **87**, 1213 (2015).

55. M. Zarea and N. Sandler, Phys. Rev. B **79**, 165442 (2009).

56. G. G. Samsonidze, R. Saito, A. Jorio, M. A. Pimenta, A. G. Souza Filho, A. Grüneis, G. Dresselhaus, and M. S. Dresselhausa, J. Nanosci. Nanotechnol. **3**, 431 (2003).

57. C. L. Kane and E. Mele, Phys. Rev. Lett. **78**, 1932 (1997).

58. C. Zhou, J. Kong, and H. Dai, Phys. Rev. Lett. **84**, 5604 (2000).

59. M. Ouyang, J. L. Huang, C. L. Cheung, and C. M. Lieber, Science **292**, 702 (2001).

60. F. L. Shyu and M. F. Lin, J. Phys. Soc. Jpn. **71**, 1820 (2002).

61. P. N. D'yachkov, Russ. J. Inorg. Chem. **63**, 55 (2018).

62. M. E. Portnoi, M. Rosenau da Costa, O. V. Kibis, and I. A. Shelykh, Int. J. Mod. Phys. B **23**, 2846 (2009).

63. R. Moradian, R. Chegel, and S. Behzad, Physica E: Low-dimens. Syst. Nanostruct. **42**, 1850 (2010).

64. R. Chegel and S. Behzad, Opt. Commun. **313**, 406 (2014).

65. R. R. Hartmann and M. E. Portnoi, IOP Conf. Ser.: Mater. Sci. Eng. **79**, 012014 (2015).

66. O. V. Kibis, M. Rosenau da Costa, and M. E. Portnoi, Nano Lett. **7**, 3414 (2007).

67. R. R. Hartmann, J. Kono, and M. E. Portnoi, Nanotechnology **25**, 322001 (2014).

68. C. T. White, J. Li, D. Gunlycke, and J. W. Mintmire, Nano Lett. **7**, 825 (2007).

69. V. A. Saroka, A. L. Pushkarchuk, S. A. Kuten, and M. E. Portnoi, J. Saudi Chem. Soc. **22**, 985 (2018).

70. H. Zheng, Z. Wang, T. Luo, Q. Shi, and J. Chen, Phys. Rev. B **75**, 165414 (2007).

71. L. A. Chernozatonskii, P. B. Sorokin, and J. W. Brüning, Appl. Phys. Lett. **91**, 183103 (2007).

72. L. A. Chernozatonskii and P. B. Sorokin, J. Phys. Chem. C **114**, 3225 (2010).

73. R. R. Hartmann, V. A. Saroka, and M. E. Portnoi, J. Appl. Phys. **125**, 151607 (2019).

74. T. Kampfrath, K. von Volkmann, C. M. Aguirre, P. Desjardins, R. Martel, M. Krenz, C. Frischkorn, M. Wolf, and L. Perfetti, Phys. Rev. Lett. **101**, 267403 (2008).

75. A. Ugawa, A. G. Rinzler, and D. B. Tanner, Phys. Rev. B **60**, 11305 (1999).

76. G. Y. Slepyan, M. V. Shuba, S. A. Maksimenko, C. Thomsen, and A. Lakhtakia, Phys. Rev. B **81**, 205423 (2010).

77. M. V. Shuba, A. G. Paddubskaya, A. O. Plyushch, P. P. Kuzhir, G. Y. Slepyan, S. A. Maksimenko, V. K. Ksenevich, P. Buka, D. Seliuta, I. Kasalynas, J. Macutkevic, G. Valusis, C. Thomsen, and A. Lakhtakia, Phys. Rev. B **85**, 165435 (2012).

78. L. Ren, Q. Zhang, C. L. Pint, A. K. Wójcik, M. Bunney, T. Arikawa, I. Kawayama, M. Tonouchi, R. H. Hauge, A. A. Belyanin, and J. Kono, Phys. Rev. B **87**, 161401 (2013).

79. J.-Y. Park, S. Rosenblatt, Y. Yaish, V. Sazonova, H. Üstünel, S. Braig, T. A. Arias, P. W. Brouwer, and P. L. McEuen, Nano Lett. **4**, 517 (2004).

80. C. Chang, Y. Huang, C. Lu, J. Ho, T. Li, and M. Lin, Carbon N. Y. **44**, 508 (2006).

81. V. A. Saroka, K. G. Batrakov, V. A. Demin, and L. A. Chernozatonskii, J. Phys.: Condens. Matter **27**, 145305 (2015).

82. L. V. Titova, C. L. Pint, Q. Zhang, R. H. Hauge, J. Kono, and F. A. Hegmann, Nano Lett. **15**, 3267 (2015).

83. J. Shaver and J. Kono, Laser Photon. Rev. **1**, 260 (2007).

84. R. Denk, M. Hohage, P. Zeppenfeld, J. Cai, C. A. Pignedoli, H. Söde, R. Fasel, X. Feng, K. Müllen, S. Wang, D. Prezzi, A. Ferretti, A. Ruini, E. Molinari, and P. Ruffieux, Nature Commun. **5**, 4253 (2014).

85. R. R. Hartmann, I. A. Shelykh, and M. E. Portnoi, Phys. Rev. B **84**, 035437 (2011).

86. R. R. Hartmann and M. E. Portnoi, Phys. Rev. A **95**, 062110 (2017).

87. A. Srivastava, H. Htoon, V. I. Klimov, and J. Kono, Phys. Rev. Lett. **101**, 087402 (2008).

88. X. He, H. Htoon, S. K. Doorn, W. H. P. Pernice, F. Pyatkov, R. Krupke, A. Jeantet, Y. Chassagneux, and C. Voisin, Nature Mater. **17**, 843 (2018).

89. W. Gao, X. Li, M. Bamba, and J. Kono, Nature Photon. **12**, 362 (2018).

90. D. Headland, T. Niu, E. Carrasco, D. Abbott, S. Sriram, M. Bhaskaran, C. Fumeaux, and W. Withayachumnankul, IEEE J. Sel. Top. Quant. Electron. **23**, 8500918 (2017).

91. H. Zhang, H. Lin, K. Sun, L. Chen, Y. Zagranyarski, N. Aghdassi, S. Duhm, Q. Li, D. Zhong, Y. Li, K. Müllen, H. Fuchs, and L. Chi, J. Amer. Chem. Soc. **137**, 4022 (2015).

92. W. Gao and J. Kono, Roy. Soc. Open Sci. **6**, 181605 (2019).